nature climate change

ARTICLES

https://doi.org/10.1038/s41558-020-0819-8

Multiple drivers of the North Atlantic warming hole

Paul Keil[1]✉, Thorsten Mauritsen[1,2], Johann Jungclaus[1], Christopher Hedemann[1], Dirk Olonscheck[1] and Rohit Ghosh[1,3]

Despite global warming, a region in the North Atlantic ocean has been observed to cool, a phenomenon known as the warming hole. Its emergence has been linked to a slowdown of the Atlantic meridional overturning circulation, which leads to a reduced ocean heat transport into the warming hole region. Here we show that, in addition to the reduced low-latitude heat import, increased ocean heat transport out of the region into higher latitudes and a shortwave cloud feedback dominate the formation and temporal evolution of the warming hole under greenhouse gas forcing. In climate model simulations of the historical period, the low-latitude Atlantic meridional overturning circulation decline does not emerge from natural variability, whereas the accelerating heat transport to higher latitudes is clearly attributable to anthropogenic forcing. Both the overturning and the gyre circulation contribute to the increased high-latitude ocean heat transport, and therefore are critical to understand the past and future evolutions of the warming hole.

The Atlantic meridional overturning circulation (AMOC) transports warm tropical water masses to the North Atlantic and, although subject to debate[1], is thought to be critical for the climate in the North Atlantic and Western Europe[2]. Climate projections show that the AMOC will weaken or potentially completely shut down in a warming climate[3,4] as a result of increased heat and freshwater fluxes in the North Atlantic[5,6]. A weakening AMOC will cause a cooling in the subpolar North Atlantic[5,7–10], reduced cloudiness over Europe[11], an increase in surface pressure over Western Europe[12,13] and a strengthened midlatitude jet[13]. Indeed, the observed cooling patch (Fig. 1a) in the North Atlantic, which has been called the warming hole (WH), was used as an indicator for a weakening AMOC[5,9]. Nevertheless, high-quality AMOC observations have only been available since 2004[14] and there is no consensus if the recently observed slow-down is part of a long-term decline or a reversal of a previous positive overturning circulation trend associated with internal variability[15].

In this study, we use the Grand Ensemble of the MPI-ESM1.1 (Max Planck Institute Earth System Model 1.1) climate model[16] to determine the nature of the relationship between the AMOC and the WH and identify additional contributing factors. The Grand Ensemble consists of 100 realizations of the historical time period (1850–2005), 100 realizations of a 150-year simulation with 1% CO_2 increase per year (here called 1pctCO_2) and a 2,000-year-long preindustrial control simulation. Whereas the historical ensemble facilitates a comparison with observations, the 1pctCO_2 ensemble serves to obtain a clear greenhouse gas forcing signal, not least because thereby any effects of aerosol forcing[17] are excluded. An overview of all the climate model configurations used in this study is given in Supplementary Table 1. The many realizations allow us to account for the internal variability of the North Atlantic sea surface temperatures (SSTs). The model reproduces the observed WH with adequate strength in the historical ensemble (Fig. 1b) and a more pronounced WH for the 1pctCO_2 simulations (Fig. 1c), compared with the observations and historical ensemble.

Atmospheric drivers

First, we disregarded the role of the ocean heat transport (OHT) and analysed the impact of atmospheric processes using three additional mixed-layer ocean simulations forced with the 1pctCO_2 scenario. Here, the OHT was prescribed and varied seasonally, but not interannually, whereby the effects of global warming on the OHT were suppressed. Nevertheless, we still found a WH in these simulations (Fig. 1d), albeit not in the form of an absolute cooling, but rather as a weaker warming. Note that the WH in the mixed-layer ocean set-up is further north than that in the fully coupled set-up and coincides with the observed WH (Fig. 1b).

To quantify the WH strength throughout different model configurations, we used the AMOC index proposed by Rahmstorf et al.[5]. However, we refer to it as warming hole index (WHI) to indicate that we use it as a measure for the WH strength rather than the AMOC strength. WHI (Methods) is calculated by subtracting the Northern Hemispheric mean surface temperature anomalies T_{NH} from the mean SST anomalies in the WH region T_{WH}:

$$\mathrm{WHI} = T_{\mathrm{WH}} - T_{\mathrm{NH}} \quad (1)$$

Quantified with this index, the mixed-layer ocean simulations can explain a substantial part of the WH as being unrelated to the changing ocean circulation (Fig. 2), the very mechanism that has been traditionally associated with the WH[5,7–9]. For example, for a global warming of 3 K, the WH warms 1.5 K less than the Northern Hemisphere warming in the mixed-layer ocean simulations and 3 K less in the Grand Ensemble. A large part of this signal is due to the land-sea warming contrast[18], but accepting this conflation enables a direct comparison to Rahmstorf et al.[5]. The land-sea warming contrast can be eliminated from the index by only considering the mean northern hemispheric SST in equation (1) as reference (Methods). The resulting WHI (Supplementary Fig. 1) continues to exhibit a weaker warming in the North Atlantic in the mixed-layer ocean simulations and it still accounts for a considerable part of the signal.

We tested whether a midlatitude cloud feedback[19] contributes to the remaining WH. To suppress the cloud feedback, three simulations with a special configuration of the MPI-ESM1.2 and one mixed-layer ocean simulation were carried out, in which the clouds were non-interactive (Methods). The cloud feedback has a small effect on the emergence of the WH (Fig. 2), but can partly explain the remaining WH in the mixed-layer ocean after excluding the

[1]Max Planck Institute for Meteorology, Hamburg, Germany. [2]Department of Meteorology, Stockholm University, Stockholm, Sweden. [3]Department of Meteorology, University of Reading, Reading, UK. ✉e-mail: paul.keil@mpimet.mpg.de

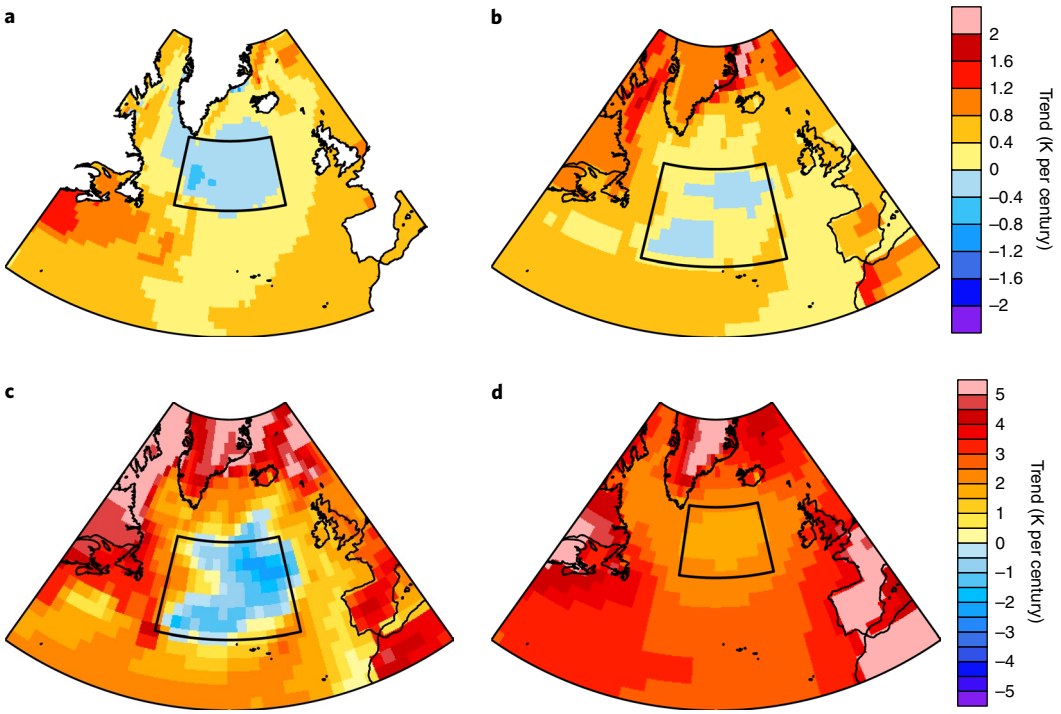

Fig. 1 | Linear surface temperature trends in the North Atlantic. a, Temperature trend for years 1870–2016 of the HadISST (Hadley Centre Sea Ice and Sea Surface Temperature) observations. **b**, Ensemble mean temperature trend for years 1850–2005 of the historical ensemble (coupled MPI-ESM1.1). **c**, Ensemble mean temperature trend for the first 80 yr of the 1pctCO$_2$ increase per year ensemble (coupled MPI-ESM1.1). **d**, Ensemble mean temperature trend for the first 80 yr of the 1pctCO$_2$ increase per year mixed-layer ocean simulations (mixed-layer ocean ECHAM6.3). The boxes indicate the regions used for the WHI (equation (1) and Fig. 2).

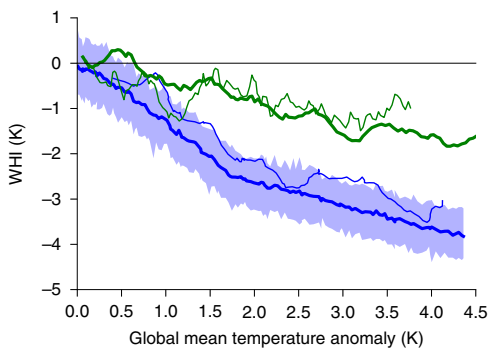

Fig. 2 | WHI for all the simulations forced by the 1pctCO$_2$ increase per year scenario. Global mean surface temperature was used as the reference variable, as the different model configurations have different rates of warming. The thick green line shows the ensemble mean of the three mixed-layer ocean simulations. The thin green line shows the 11-yr running mean of the single realization of the mixed-layer ocean simulation with non-interactive clouds. The thick blue line shows the ensemble mean of the coupled Grand Ensemble simulations and the blue shading indicates the 5th and 95th percentiles. The thin blue line represents the ensemble mean of the three coupled simulations with non-interactive clouds. The regions used for the WHI are shown as boxes in Fig. 1.

land–sea warming contrast (Supplementary Fig. 1). Enhanced evaporative cooling associated with increased surface winds also contributes to the WH in the mixed-layer ocean simulation (not shown). We found that the cloud feedback is enhanced in the fully coupled simulations[20], as the strong surface cooling increases regional surface pressures[12,13] (Supplementary Fig. 2) and thereby produces more low-level clouds[11] (Supplementary Fig. 3). Over longer timescales, the non-interactive cloud simulations in the fully coupled case have a distinctly weaker WH compared with that of the Grand Ensemble (Supplementary Fig. 4). Thus, the cloud feedback makes a small but discernible contribution to the WH in MPI-ESM1.1 and the magnitude of the WH in turn strengthens the regionally cooling cloud feedback.

WH–AMOC relationship

Having presented that atmospheric processes contribute to the WH, we now focus on the role of OHT because we found that the bulk of the WH signal in the coupled simulations is associated with the ocean circulation (Fig. 1). Other studies have already established that a relation between WHI and AMOC strength at 26° N exists[5,9], for example, Rahmstorf et al.[5] derived a linear relationship between the AMOC strength and the WHI of 2.3 Sv K^{-1} (Sv = 10^6 m^3 s^{-1}) from an earlier version of the MPI-ESM with RCP8.5 (representative concentration pathway 8.5) future global warming scenario. For MPI-ESM1.1, we found that the relationship depends on the forcing evolution (Fig. 3) and even changed with time, as is the case in the 1pctCO$_2$ ensemble: for a given WH temperature anomaly; the AMOC changed five times less in the forced simulation compared with the control simulation. The historical ensemble incorporates both of these WH–AMOC relationships, which we demonstrated by separating the forced signal as represented by the ensemble mean from the internal variability calculated as deviations from the ensemble mean (Methods). The latter resembles the control simulation and the forced signal was even weaker than that found in the 1pctCO$_2$ ensemble—more than ten times less than that for internal variability. Volcanic and anthropogenic aerosol forcing[17] might be responsible for some of the differences between the forced response of the historical ensemble and the 1pctCO$_2$ ensemble, as the latter

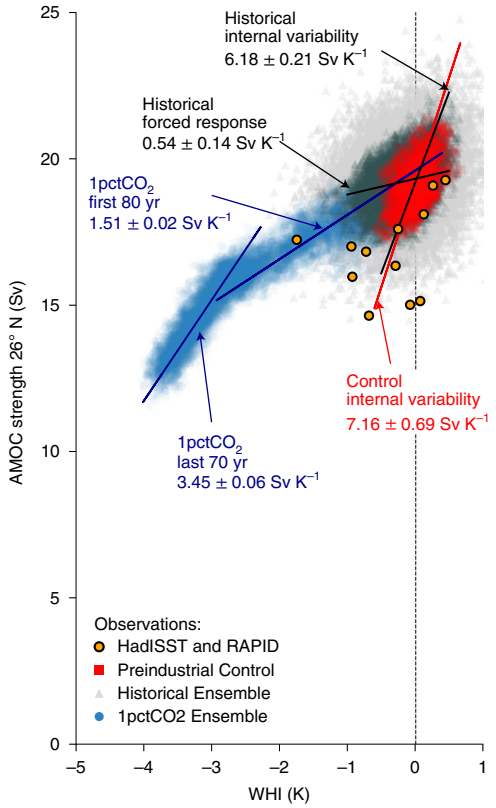

Fig. 3 | Relationship between AMOC strength and the WHI for various simulations and observations. AMOC strength is derived from the AMOC streamfunction at a 1,000-m depth and 26° N. All the values are 11-yr running means, except for the observations and the light-grey triangles, which represent the yearly means of the historical ensemble for comparison with the observations. Blue circles show values from all 100 ensemble members of the 1pctCO$_2$ simulation. The corresponding regression lines are shown in dark blue for the first 80 and last 70 yr, respectively. Dark grey triangles show the 100-ensemble historical simulation and the black lines show the corresponding regressions based on ensemble mean values (forced response) and on deviations from the ensemble mean (internal variability). The values from the 2,000-yr control simulation are shown as red squares and the corresponding regression line in red. All the regressions are orthogonal regressions, which take errors in both variables into account (Methods). The errors of the slopes were calculated with the 99% confidence interval using a Student's *t*-test. The orange dots encircled by black represent observations. The AMOC strength was taken from the RAPID array and WHI (equation (1)) was calculated with HadISST and HadCRUT (Hadley Centre and Climatic Research Unit) data.

does not include any of these forcings. We note the AMOC in the historical simulations (19.1 Sv on average for the years 1990–2005) is somewhat stronger compared with the observations (16.9 Sv on average for the years 2004–2018), but that the spread in the observations is similar to that of the historical ensemble, which suggests the relationship found in the model is in accordance with the sparse observations. Despite these different relationships, the original conversion factor of 2.3 Sv K^{-1} reproduces the temporal variability of the AMOC to the first order[5] and our results confirm that the internal variability of the WH temperatures is, indeed, closely connected with the low-latitude AMOC (Fig. 3).

High-latitude circulation changes

In the mean state, the OHT converges at the WH latitudes, as the heat import from lower latitudes outweighs the export to the Labrador and Nordic Seas. The excess heat is lost to the atmosphere. Under the 1pctCO$_2$ forcing, a heat budget analysis (Methods) reveals that the convergence of OHT decreases in the North Atlantic (Supplementary Fig. 5), as in most climate models[8], especially during the first 80 years in this case. Simultaneously, as the WH becomes stronger, the surface heat loss decreases, which results in an approximately constant ocean heat content in the North Atlantic. In this heat budget, the cooling in the WH is compensated by the warming around it, whereas the global ocean heat content increase is faster (Supplementary Fig. 5c) . The surface fluxes in the mixed-layer ocean simulations do not behave as in the fully coupled case here, which emphasizes that the behaviour of the surface fluxes is largely a response to the OHT changes. The shortwave part of the surface fluxes affected by the cloud feedback discussed above is a separate case. After approximately 80 years, the OHT convergence decrease decelerates and the CO$_2$ forcing dominates the heat flow into the region, which causes an increase in ocean heat content.

To better understand the change of the OHT under global warming, we examined the advective OHT throughout the North Atlantic basin and decomposed it into its respective contributions from the AMOC and gyre circulations (Methods). Whereas heat import from the south, mainly associated with the AMOC, into the WH latitudes decreases linearly in the 1pctCO$_2$ experiment, the OHT out of the region polewards increases simultaneously during the first 80 years (Fig. 4a). The increased OHT to the Arctic contributes to the reduced heat convergence at the latitudes where the WH is situated (Fig. 4b). Furthermore, we found that this enhanced OHT is caused by both an increase in the OHT associated with a changing gyre circulation[10], which has hardly been explored yet[21], as well as the high-latitude AMOC (Fig. 4b and Supplementary Fig. 6). Neither of these processes show a robust relationship to WH temperatures in the control simulation, but they emerge once the forcing is applied (Supplementary Figs. 7 and 8). The increase of OHT to higher latitudes stalls after about 80 years of simulation time and gradually decreases thereafter (Fig. 4a). This is reflected in the change of the AMOC–WHI relationship after 80 years (Fig. 3) and explains the temporal evolution of the WH (Fig. 2). The relative increase in anomalous OHT at the northern compared to the southern boundary could reflect changes in the circulation, temperature or both[21]. Although we did not include this separation in our analyses, we found clear evidence for an enhanced overturning and subpolar gyre circulation, a feature that is elaborated further in a separate paper (R.G., manuscript in preparation).

Consequently, the long-term evolution of the WH in a forced scenario, in contrast to internal variability, is driven by a multitude of factors: OHT changes at low and high latitudes associated with both the overturning and gyre circulation along with atmospheric processes (Fig. 5). Although reduced vertical mixing could also contribute to surface cooling[8], we found that the vertical extent of the cooling is much deeper than the mixed layer and therefore can be excluded as a main driver of the WH in our model (Supplementary Fig. 9). Recently, Gervais et al.[10] connected the formation of the WH to an import of cold near-surface water masses from the Labrador Sea and a reduced deep western boundary current. These proposed mechanisms are consistent with our results, because the import of cold water masses would be reflected in the gyre-related heat transports, and the reduced deep western boundary current is represented by a reduced overturning at lower latitudes.

In the historical ensemble, individual ensemble members disagree on the evolution of the low-latitude OHT and as a result the ensemble mean does not show any significant change (Fig. 4c). However, the WH robustly appears in all realizations of the historical ensemble and it has been shown that the historical WH precedes the AMOC decline[7,10]. In contrast, all the members agree on an increase of high-latitude OHT across the ensemble, which results in a decreased heat convergence at the latitudes of the WH. Whereas

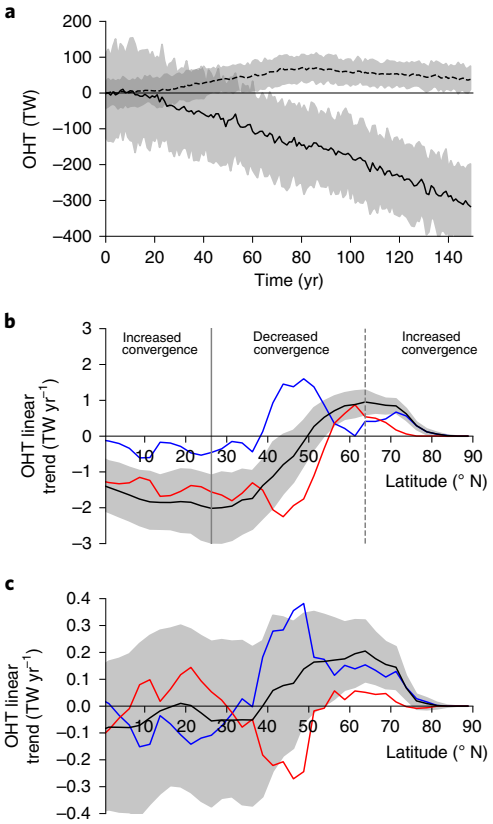

Fig. 4 | North Atlantic OHT changes in the Grand Ensemble. a, Evolution of the Atlantic heat transport anomalies relative to the preindustrial control simulation at 26.25° N (black solid line) and 63.75° N (black dashed line) in the 1pctCO$_2$ experiment. Shading represents the 5th and 95th percentiles of the ensemble. **b**, Ensemble mean linear trends of the Atlantic OHT for the first 80 yr in the 1pctCO$_2$ ensemble. Shading represents the 5th and 95th percentiles of the total heat transport trend (black line) of the ensemble. Linear trends of the AMOC and gyre components are shown in red and blue, respectively. The latitudes chosen in **a** are those at which the strongest positive and negative trends of heat transport occur and thus they separate regions of increased heat convergence and divergence, as indicated by the corresponding continuous and dashed vertical lines in **b**. **c**, Ensemble mean linear trends of the Atlantic OHT in the historical ensemble from 1850 to 2005. The colour lines and grey shading are as in **b**.

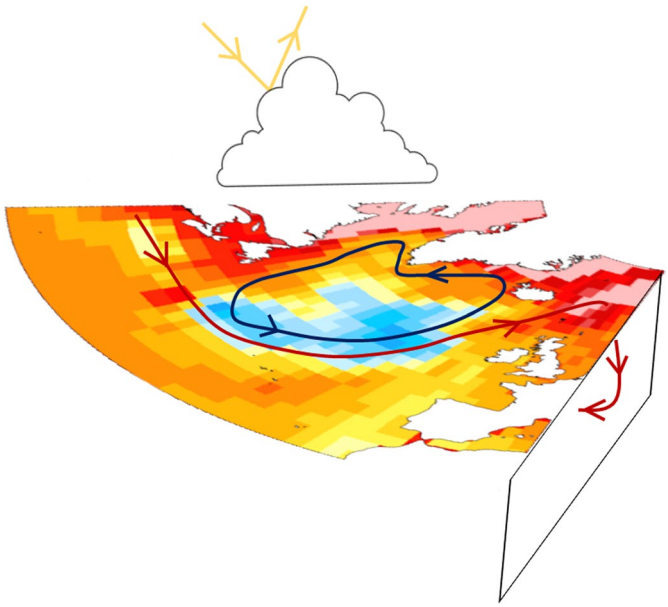

Fig. 5 | Schematic illustration of the drivers of the WH. The AMOC is indicated by red arrows, the gyre circulation by blue arrows and cloud feedback in the form of reflected shortwave radiation by yellow arrows. Shading represents the surface temperature trend of the 1pctCO$_2$ increase per year ensemble.

internal variability of the WH temperatures in individual realizations is likely to be influenced by the low-latitude AMOC[5,9], the long-term forced SST trend over the historical period (Fig. 1b) can only be attributed to the high-latitude OHT changes.

The exact shape of the temperature pattern, including the warming off the North American east coast (Fig. 1a), has been linked to the mechanism of a declining AMOC and therefore suggested to be an important indicator for a climate model's ability to produce a realistic ocean circulation response and WH[9]. This warming patch is not reproduced in the historical ensemble mean (Fig. 1b), which might be due to the model resolution[9,22]. However, the details of the temperature pattern in the historical ensemble (and the observations) are greatly influenced by internal variability and therefore show considerable variation throughout the ensemble. As the AMOC south of 50° N does not show robust changes in the historical period (Fig. 1c), it is not surprising that the warming patch is not a robust feature of the historical WH. For stronger forcing. the warming patch appears in the ensemble mean (Fig. 1c) along with the emerging trend of the AMOC decline (Fig. 1b).

It can be revealing to inspect how the low- and high-latitude OHTs are linked in natural variability and under forcing[21]: in the absence of externally forced global warming, the OHTs at lower and higher latitudes are in phase (Fig. 6), which thereby results in a large magnitude of the AMOC–WH relationship. In the 1pctCO$_2$ experiment, however, this breaks down such that heat import from the south decreases and export to the north increases at the same time, and as a consequence the AMOC–WH relationship also changes substantially under greenhouse gas forcing. After the 80-year mark the relationship between low- and high-latitude OHT returns to its preindustrial in-phase relationship.

Summary and discussion

We used the MPI-ESM1.1 in the low-resolution (LR) setting to investigate the WH, but the characteristics of the SST pattern[8], as well as the related circulation changes[21], vary throughout climate models. This may be related to model resolution or different formulations of the physical processes. We acknowledge that our study does not span the full range of a multimodel assessment. For example, although we exclude vertical mixing as a driver for the WH in this study, it has been shown that this process is important in some models[8]. In contrast, the disadvantages of studies that use many models, but a small amount of realizations, is that the spread due to model biases cannot be separated from the spread related to internal variability, which is especially important in the North Atlantic. Here we can precisely account for internal variability, which only leaves the model bias as an error source. In addition, conducting the experiments with locked clouds and a mixed-layer ocean in the same model family makes the results comparable.

Recent attempts to attribute the emergence of the WH predominately to an AMOC slow-down[5,8,9] overlook the multitude of physical mechanisms that control the North Atlantic SST response to forced warming (Fig. 5). Further, even if a slow-down is recorded in direct measurements of the overturning circulation[14], it is futile to attribute this signal to anthropogenic forcing, because the AMOC natural variability dominates the relatively weakly forced signal during the observational period[15]. Nevertheless, the surface-temperature WH

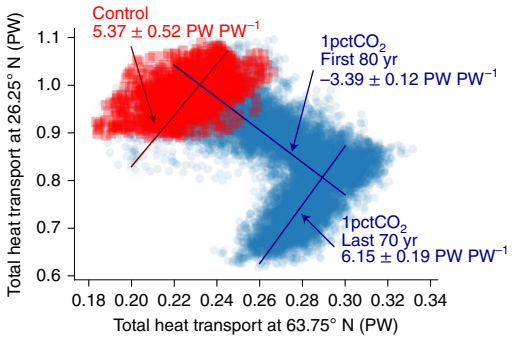

Fig. 6 | Relationship of the total advective heat transport at low and high latitudes in the Grand Ensemble. The chosen latitudes are those from Fig. 4a. Red squares indicate the preindustrial control simulation and blue circles indicate all 100 ensemble members of the 1pctCO$_2$ simulations. All the values are 11-yr running means. The regression lines for the 1pctCO$_2$ ensemble represent the first 80 yr and the last 70 yr, respectively. The errors of the slopes were calculated with the 99% confidence interval using Student's *t*-test.

has been reliably observed and is most probably a response to greenhouse gas forcing, not least because it is present in all the historical ensemble members of the MPI-ESM1.1 Grand Ensemble. Thus, the WH and its impacts on local and global atmospheric circulation[12,13] can be attributed to anthropogenic forcing even if the low-latitude AMOC decline cannot. According to our model, the currently observed WH is probably related to high-latitude ocean circulation changes, which precede the low-latitude changes[7,10] (Fig. 4c). Under stronger greenhouse gas forcing in the future, the low-latitude AMOC changes will also contribute to the WH as one of multiple drivers, but to infer the AMOC strength from a WHI[5,9] is error prone. Furthermore, by inducing enhanced low-level cloudiness (Supplementary Fig. 3), the North Atlantic ocean circulation could already be playing an active role in temporarily dampening global warming through the so-called SST pattern effects[23,24]. It would be helpful if, in future discussions, the impacts of the WH are separated from its underlying causes, which involve both atmospheric processes and an enhanced northward heat transport out of the region, and therefore extend beyond that of a simple AMOC slow-down.

Online content

Any methods, additional references, Nature Research reporting summaries, source data, extended data, supplementary information, acknowledgements, peer review information; details of author contributions and competing interests; and statements of data and code availability are available at https://doi.org/10.1038/s41558-020-0819-8.

Received: 16 May 2019; Accepted: 16 May 2020;
Published online: 29 June 2020

References

1. Seager, R. et al. Is the gulf stream responsible for Europe's mild winters? *Q. J. R. Meteorol. Soc.* **128**, 2563–2586 (2002).
2. Kaspi, Y. & Schneider, T. Winter cold of eastern continental boundaries induced by warm ocean waters. *Nature* **471**, 621–624 (2011).
3. Stocker, T. F. & Wright, D. G. Rapid transitions of the ocean's deep circulation induced by changes in surface water fluxes. *Nature* **351**, 729–732 (1991).
4. Rahmstorf, S. Bifurcations of the Atlantic thermohaline circulation in response to changes in the hydrological cycle. *Nature* **378**, 145–149 (1995).
5. Rahmstorf, S. et al. Exceptional twentieth-century slowdown in Atlantic Ocean overturning circulation. *Nat. Clim. Change* **5**, 475–480 (2015).
6. Sévellec, F., Fedorov, A. V. & Liu, W. Arctic sea-ice decline weakens the Atlantic meridional overturning circulation. *Nat. Clim. Change* **7**, 604–610 (2017).
7. Drijfhout, S., Van Oldenborgh, G. J. & Cimatoribus, A. Is a decline of AMOC causing the warming hole above the North Atlantic in observed and modeled warming patterns? *J. Clim.* **25**, 8373–8379 (2012).
8. Menary, M. B. & Wood, R. A. An anatomy of the projected North Atlantic warming hole in CMIP5 models. *Clim. Dynam.* **50**, 3063–3080 (2018).
9. Caesar, L., Rahmstorf, S., Robinson, A., Feulner, G. & Saba, V. Observed fingerprint of a weakening Atlantic Ocean overturning circulation. *Nature* **556**, 191–196 (2018).
10. Gervais, M., Shaman, J. & Kushnir, Y. Mechanisms governing the development of the North Atlantic warming hole in the CESM-LE future climate simulations. *J. Clim.* **31**, 5927–5946 (2018).
11. Laurian, A., Drijfhout, S., Hazeleger, W. & van den Hurk, B. Response of the Western European climate to a collapse of the thermohaline circulation. *Clim. Dynam.* **34**, 689–697 (2010).
12. Haarsma, R. J., Selten, F. M. & Drijfhout, S. S. Decelerating Atlantic meridional overturning circulation main cause of future West European summer atmospheric circulation changes. *Environ. Res. Lett.* **10**, 094007 (2015).
13. Gervais, M., Shaman, J. & Kushnir, Y. Impacts of the North Atlantic warming hole in future climate projections: mean atmospheric circulation and the North Atlantic jet. *J. Clim.* **32**, 2673–2689 (2019).
14. Smeed, D. et al. Observed decline of the Atlantic meridional overturning circulation 2004–2012. *Ocean Sci.* **10**, 29–38 (2014).
15. Jackson, L. C., Peterson, K. A., Roberts, C. D. & Wood, R. A. Recent slowing of Atlantic overturning circulation as a recovery from earlier strengthening. *Nat. Geosci.* **9**, 518–522 (2016).
16. Maher, N. et al. The Max Planck Institute Grand Ensemble—enabling the exploration of climate system variability. *J. Adv. Model. Earth Syst.* **11**, 2050–2069 (2019).
17. Booth, B. B., Dunstone, N. J., Halloran, P. R., Andrews, T. & Bellouin, N. Aerosols implicated as a prime driver of twentieth-century North Atlantic climate variability. *Nature* **484**, 228–232 (2012).
18. Sutton, R. T., Dong, B. & Gregory, J. M. Land/sea warming ratio in response to climate change: IPCC AR4 model results and comparison with observations. *Geophys. Res. Lett.* **34**, L02701 (2007).
19. Ceppi, P., McCoy, D. T. & Hartmann, D. L. Observational evidence for a negative shortwave cloud feedback in middle to high latitudes. *Geophys. Res. Lett.* **43**, 1331–1339 (2016).
20. Trossman, D., Palter, J., Merlis, T., Huang, Y. & Xia, Y. Large-scale ocean circulation–cloud interactions reduce the pace of transient climate change. *Geophys. Res. Lett.* **43**, 3935–3943 (2016).
21. Oldenburg, D., Armour, K. C., Thompson, L. & Bitz, C. M. Distinct mechanisms of ocean heat transport into the Arctic under internal variability and climate change. *Geophys. Res. Lett.* **45**, 7692–7700 (2018).
22. Jungclaus, J. et al. Characteristics of the ocean simulations in the Max Planck Institute Ocean Model (MPIOM) the ocean component of the MPI-Earth system model. *J. Adv. Model. Earth Syst.* **5**, 422–446 (2013).
23. Senior, C. A. & Mitchell, J. F. The time-dependence of climate sensitivity. *Geophys. Res. Lett.* **27**, 2685–2688 (2000).
24. Armour, K. C., Bitz, C. M. & Roe, G. H. Time-varying climate sensitivity from regional feedbacks. *J. Clim.* **26**, 4518–4534 (2013).

Methods

The Grand Ensemble. Large ensembles of simulations, referred to as the Grand Ensemble[16], carried out with the MPI-ESM1.1 (ref. [25]) form the basis of this study. An overview of all the used climate model data is given in Supplementary Table 1, which includes the additional special simulations described below. All the ensemble members of the Grand Ensemble are simulations with the low-resolution version MPI-ESM1.1, which has a T63/1.9° horizontal resolution in the atmosphere and an approximately 1.5° horizontal resolution in the ocean. The historical experiments were carried out using natural and anthropogenic forcing derived from observations. Anthropogenic aerosols were included, but only the direct aerosol effect on the radiation was simulated. The 1pctCO_2 increase per year experiment was solely forced by the increase in CO_2 concentration, which doubles every 70 yr.

Mixed-layer ocean simulations. Three mixed-layer ocean (or 'slab' ocean) simulations were performed using ECHAM-6.3.04[25] with a 1pctCO_2 increase per year forcing and a corresponding control simulation. The mixed-layer ocean did not include a circulation scheme and basically acts as a heat capacity with vertically uniform temperature, which mimics the well-mixed upper ocean that interacts with the atmosphere. The uniform depth of the mixed layer was set to 50 m. A prescribed OHT functioned as a substitute for the OHT associated with the large-scale ocean circulation beyond the mixed layer. This prescribed heat transport varies seasonally, but not interannually, whereby the effects of global warming on the OHT are suppressed. Overall, the set-up is similar to that implemented in Clement et al.[26].

Simulations with non-interactive clouds. To assess atmospheric impacts on the WH, we performed additional experiments with the model branch MPI-ESM1.2.00p3 fixvar in the LR setting, in which the clouds are non-interactive: a control simulation and three simulations with 1pctCO_2 increase per year forcing. In these non-interactive cloud simulations, we decoupled the radiative effects of clouds from the rest of the model by reading random cloud fields into the radiation scheme at every 2-h radiation call. The random cloud fields were created by shuffling the cloud fields produced by a regular preindustrial control experiment. The method follows that applied by Olonscheck et al.[27]. We additionally performed a mixed-layer ocean experiment with the atmosphere component of MPI-ESM1.1 found in the branch ECHAM-6.3.02p2_fixvar with non-interactive clouds, with one control and one forced simulation, using the same OHT representation as above. However, in this case the cloud fields of only 1 yr of the control experiment were implemented into the radiation scheme without randomization. This distinction is not deemed important for the purposes here, which are to study the mean state response.

WHI. We adapted the AMOC index from Rahmstorf et al.[5], here WHI (equation (1)), as it is used as a measure of WH strength in this study. For all the climate model configurations, we calculated temperature anomalies T_{WH} as the mean surface temperature anomaly in the WH region and T_{NH} as the mean Northern Hemisphere surface temperature anomaly with respect to the control simulations. Temperature anomalies of the HadISST data[28] were calculated with respect to the 1880–1910 period. This inconsistency slightly affects the comparability of the observed WH with the climate model WH, but is beneficial when comparing the WH among different model configurations. As the spatial position of the WH varies throughout the model configurations and the observational dataset, different regions for the calculation of the WHI were used, as indicated in Fig. 1. The alternative WHI, WHI_{SST}, which was also considered in Rahmstorf et al.[5], the mean Northern Hemispheric SST, SST_{NH}, was used as reference:

$$WHI_{SST} = T_{WH} - SST_{NH} \quad (2)$$

We decided on using Northern Hemispheric SSTs instead of global SSTs used by Caesar et al.[9] as the Southern Hemispheric SSTs show a much weaker warming overall and therefore dampen the WH signal.

Orthogonal regression. We use orthogonal regression, also known as total least squares regression, to evaluate the relationship between two variables, such as WHI and AMOC strength. Thereby, the error in both variables is minimized. Slopes and their standard errors were calculated with the python scipy.odr package. Orthogonal regression is, however, not scale invariant, which is especially relevant for Supplementary Figs. 7 and 8. In these instances, the OHT was converted into units of picowatts (10^{15} W) before the regression to adjust the scale to that of the WHI. We perform two regressions (Fig. 3) for the historical ensemble—one based on ensemble mean values and one based on the deviations from the ensemble mean. The former is a regression of the ensemble mean values of the WHI and the AMOC streamfunction over the years 1850–2005. For the latter, we first calculated the deviations of the WHI and the AMOC streamfunction for every ensemble member by subtracting the ensemble mean. The regression then takes into account deviations of every ensemble member and every timestep.

Heat budget analysis. We conducted a heat budget analysis using the heat content, OHT and the surface fluxes. For a single grid cell, annual averages of the heat content H were calculated from the annual averages of the potential temperature θ, specific heat capacity c, density of seawater ρ (assumed constant) and volume of the grid cell V:

$$H = \rho c \theta V \quad (3)$$

The OHT in this case also includes contributions from the parameterized physics (eddy-induced transport and diffusion), as well as the resolved advective OHT. The surface fluxes include contributions from long-wave and short-wave radiation, as well as latent and sensible heat fluxes, but not any minor processes, such as the heat of precipitating water. To obtain a closed budget, the OHT needs to be calculated along straight lines of the native grid bordered by land masses, which is why we chose the area illustrated in Supplementary Fig. 5 and not the WHI area (Fig. 1) or the area of decreased OHT convergence (Fig. 4).

Heat transports associated with AMOC and gyre circulation. To evaluate the proportion in which the AMOC and gyre circulation contribute to the OHT, we followed the measures used by Griffies et al.[29]. The y-direction heat transport in a grid cell with edges dx, dy and dz can be calculated as:

$$\rho v \theta dx dz = V \theta dx \quad (4)$$

Here v represents the meridional velocity. $V = \rho v dz$ is introduced so that Vdx can be interpreted as the meridional mass transport. The heat transport in the x direction was calculated accordingly. The basin-wide advective heat transport (HT) in the y direction was calculated as the sum along the x direction and vertical sum of the transport of potential temperature:

$$HT = \sum_i \sum_k \theta V dx \quad (5)$$

For the zonal sum, lines on the native grid that follow the latitudes were constructed (which resulted in a 'zigzag' path). Thus, the zonal sum also includes advective heat transport in the x direction of grid cells along the constructed lines. Transport across such a line and potential temperature were decomposed into a zonal mean (indicated by the brackets in equation (6)) and its deviations (indicated by the asterisks in equation (7)). From this set-up, we can derive two expressions that represent the AMOC and gyre circulation systems.

$$AMOC = [\theta][V] \quad (6)$$

$$Gyre = \theta^* V^* \quad (7)$$

The remaining terms are considered too small to be important.

Data availability

HadCRUT4 data were provided by the UK Met Office Hadley Centre (http://www.met-office.gov.uk/hadobs/hadcrut4/), as well as HadISST data (https://www.metoffice.gov.uk/hadobs/hadisst/). Data from the RAPID-WATCH MOC monitoring project are freely available from www.rapid.ac.uk/rapidmoc funded by the Natural Environment Research Council. The Grand Ensemble is publicly available at ESGF (https://esgf-data.dkrz.de/projects/esgf-dkrz/). The special simulations are available on request from the corresponding author.

Code availability

An archive with the bash, python and NCL scripts used to conduct the calculations that underlie this study and reproduce the figures is archived by the Max Planck Institute for Meteorology and can be accessed from the public repository of the Max Planck Society, https://pure.mpg.de/pubman/faces/ViewItemOverviewPage.jsp?itemId=item_3213979.

References

25. Mauritsen, T. et al. Developments in the MPI-M Earth System Model version 1.2 (MPI-ESM1. 2) and its response to increasing CO_2. *J. Adv. Model. Earth Syst.* **11**, 998–1038 (2019).
26. Clement, A. et al. The Atlantic multidecadal oscillation without a role for ocean circulation. *Science* **350**, 320–324 (2015).
27. Olonscheck, D., Mauritsen, T. & Notz, D. Arctic sea-ice variability is primarily driven by atmospheric temperature fluctuations. *Nat. Geosci.* **12**, 430–434 (2019).
28. Rayner, N. et al. Global analyses of sea surface temperature, sea ice, and night marine air temperature since the late nineteenth century. *J. Geophys. Res. Atmos.* **108**, 4407 (2003).
29. Griffies, S. M. et al. OMIP contribution to CMIP6: experimental and diagnostic protocol for the physical component of the Ocean Model Intercomparison Project. *Geosci. Model Dev.* **9**, 3231 (2016).

Acknowledgements

The study benefited from comments by B. Stevens, H. Haak and C. Li. T.M. received funding from the European Research Council (ERC) Consolidator Grant 770765 and the European Union's Horizon 2020 Program Grant agreement 820829. Computational resources were made available by Deutsches Klimarechenzentrum (DKRZ) through support from the Bundesministerium für Bildung und Forschung (BMBF) and by the Swiss National Supercomputing Centre (CSCS). J.J. acknowledges support through BMBF under grants 01LP1517B (MiKliP) and 03F0729D (RACE).

Author contributions

The original idea for this study was conceived by T.M., and P.K. carried out the bulk of the analysis. All the authors contributed to developing the methodology and writing the manuscript.

Competing interests

The authors declare no competing interests.

Additional information

Supplementary information is available for this paper at https://doi.org/10.1038/s41558-020-0819-8.

Correspondence and requests for materials should be addressed to P.K.

Peer review information *Nature Climate Change* thanks Melissa Gervais and the other, anonymous, reviewer(s) for their contribution to the peer review of this work.

Reprints and permissions information is available at www.nature.com/reprints.